the aid of the continuation software package XPP AUT [40] is displayed in Fig. 17. The top-left panel shows the norm of the real part of the vector $[z_1, z_2]$ as a function of the excitation parameter, μ. The bottom-right panel displays the corresponding μ-path in the $(\tilde{\sigma}, \tilde{\mu})$-plane.

4.3 The effect of the cubic imaginary term

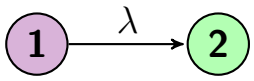

$$\begin{aligned} \dot{z}_1 &= (\mu + i\omega) z_1 - |z_1|^2 z_1 \\ \dot{z}_2 &= \big((\mu + \varepsilon) + i(\omega + \sigma)\big) z_2 - (1 + \gamma\, i)|z_2|^2 z_2 - \lambda z_1. \end{aligned} \tag{46}$$

Figure 18: A schematic diagram of a two-cell feed-forward network with Stuart-Landau cells with inhomogeneities in the natural frequency, the excitation parameter, and the cubic nonlinearity, represented by σ, ε, and γ, respectively.

In this section, we consider the case where the complex cubic nonlinearity coefficient, γ, is nonzero. Figure 18 illustrates this case. A near-identity transformation of the form $z_2 = \tilde{z}_2\left(1 + i\frac{\gamma}{\mu+\varepsilon}|\tilde{z}_2|^2\right)$ eliminates the complex coefficient γ in the cubic nonlinearity, but introduces an $O(|z_2|^5)$ term. If we were only interested in bifurcations when μ changes from a negative to a small positive value, these higher-order terms would have an insignificant effect; they are not included in the normal form. By contrast, we aim to investigate the dynamics of system (32) across a broad range of parameter values, thereby making the effect of these higher-order terms substantial. Therefore, we retain the γ-term and examine system (32) using the approach employed for $\gamma = 0$.

We assume that the first cell in Eq. (46) is settled onto its periodic attractor $z_1(t) = \sqrt{\mu} e^{i\omega t}$. Then the ODE for the second cell in Eq. (46) is

$$\dot{z}_2 = (\mu + \varepsilon + i(\omega + \sigma)) z_2 - (1 + i\gamma)|z_2|^2 z_2 - \lambda\sqrt{\mu} e^{i\omega t}. \tag{47}$$

The motion of the second cell in the co-rotating frame is represented by a new variable u that relates to z_2 via $z_2 = u e^{i\omega t}$. The ODE for u is:

$$\dot{u} = (\mu + \varepsilon + i\sigma) u - (1 + i\gamma)|u|^2 u - \lambda\sqrt{\mu}. \tag{48}$$

4.3.1 The reduced system analysis

Let $\mu > 0$. We consider the case $\mu + \varepsilon > 0$. The case $\mu + \epsilon \le 0$ can be analyzed using the same variable changes as those used for this case when $\gamma = 0$.

The time rescaling, the variable change, and parameter redefinition given by

$$\tau = \lambda\sqrt{\frac{\mu}{\mu + \varepsilon}}, \quad u = v\sqrt{\mu + \varepsilon}, \quad \tilde{\mu} = \frac{\mu + \varepsilon}{\lambda}\sqrt{\frac{\mu + \varepsilon}{\mu}}, \quad \tilde{\sigma} = \frac{\sigma}{\lambda}\sqrt{\frac{\mu + \varepsilon}{\mu}}, \tag{49}$$

result in the following ODE for the new variable v:

$$\dot{v} = \tilde{\mu}\left(1 - |v|^2\right) v + i\left(\tilde{\sigma} - \tilde{\mu}\gamma|v|^2\right) v - 1. \tag{50}$$

The corresponding system of ODEs for the real and imaginary parts of v is:

$$\begin{aligned} v_R &= \tilde{\mu}\left(1 - |v|^2\right) v_R - \left(\tilde{\sigma} - \tilde{\mu}\gamma|v|^2\right) v_I - 1, \\ v_I &= \tilde{\mu}\left(1 - |v|^2\right) v_I + \left(\tilde{\sigma} - \tilde{\mu}\gamma|v|^2\right) v_R. \end{aligned} \tag{51}$$

The equilibria of Eq. (51) are the solutions of the following equation for $|v|^2$:

$$\tilde{\mu}^2\left(1 - |v|^2\right)^2 |v|^2 + \left(\tilde{\sigma} - \tilde{\mu}\gamma|v|^2\right)^2 |v|^2 = 1. \tag{52}$$

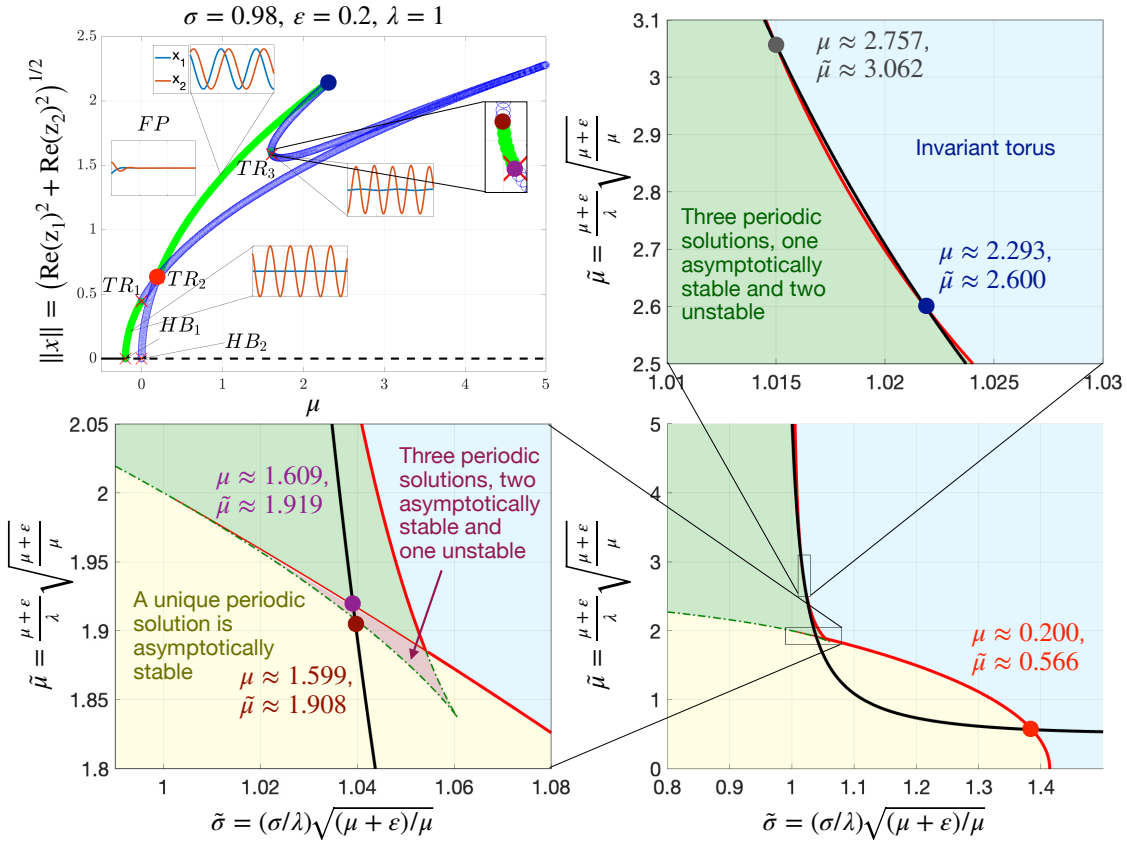

Figure 17: A bifurcation diagram (top left) of the response of Eq. (32) as a function of the excitation parameter μ. All other parameter values are shown in the figure. Green (blue) circles depict stable (unstable) oscillations that arise via Hopf bifurcations, labeled HB_1 and HB_2. Tori bifurcations, which correspond to secondary Hopf bifurcations, are labeled TR_1 and TR_2. They lead to quasi-periodic motion. The corresponding μ-path is shown in the bottom right, and two zoom-ins of its traverse through the pink region with two asymptotically stable periodic solutions and its re-entry of the green region are shown in the zoom-ins. As μ increases, starting with negative values, a Hopf bifurcation, labeled HB_1, occurs at $\mu = -\varepsilon = -0.2$. This bifurcation brings cell two to oscillate at frequency $\omega + \sigma$, while cell one is at rest, and to follow the green branch in the interval $-0.2 < \mu < 0$. Another Hopf bifurcation, HB_2, at $\mu = 0$ gives rise to limit-cycle oscillations of cell one at frequency ω. Since cell two is already oscillating at a different frequency, the combined effect is a torus bifurcation, TR_1, leading to quasi-periodic oscillations. At $\mu > 0$, the events on the $(\mu, \|x\|)$-bifurcation diagram on the top-left panel can be understood by following the corresponding μ-path on the $(\tilde{\mu}, \tilde{\sigma})$ phase diagram on the bottom-right panel. The μ-path enters the yellow region at the point marked by a bright red dot and labeled by TR_2 in the $(\mu, \|x\|)$-diagram. The torus attractor disappears at this point, giving rise to a periodic attractor represented by the green branch starting at the bright red dot and ending at the dark blue dot in the top-left panel. The μ-path traverses the pink region zoomed in on the bottom-left panel, where two periodic attractors exist. The second periodic solution with smaller amplitude in the second cell lies on the slanted-j-shaped branch in the top-left panel, with a tiny stable interval zoomed in on in the inset. The μ-path enters the green region in the bottom-right panel, then leaves it, and re-enters it again. This excursion to the blue region is zoomed in on the top-right panel. The green branch at the top-left ends at the exit point: XPP AUT has not found its continuation. The traverse of the μ-path through the pink and green regions is marked by the existence of three periodic phase-locked solutions lying on the green and the slanted-j-shaped branches in which both cells oscillate at frequency ω. The other blue branch emanating from the point TR_2 corresponds to the unstable periodic solution where cell one is at rest and cell two oscillates at frequency $\omega + \sigma$.

At any fixed $\tilde{\mu} > 0$, $\tilde{\sigma} \in \mathbb{R}$, and $\gamma \in \mathbb{R}$, Eq. (52) has at least one solution $|v|^2$, and each solution of Eq. (52) uniquely determines v_R and v_I from Eq. (51).

Eq. (52) defines a family of slanted ellipses in the $(\tilde{\sigma}, \tilde{\mu})$-plane at any fixed γ. The semiaxes directions and magnitudes are, respectively, the eigenvectors and the reciprocals of the square roots of the eigenvalues of the matrix

$$M\left(|v|^2, \gamma\right) = \begin{bmatrix} |v|^2 & -\gamma|v|^4 \\ -\gamma|v|^4 & \left(1-|v|^2\right)^2 |v|^2 + \gamma|v|^6 \end{bmatrix}. \tag{53}$$

As $|v|^2 \to \pm 1$, the ellipses degenerate into two parallel lines $\tilde{\sigma} - \tilde{\mu}\gamma = \pm 1$ in the $(\tilde{\sigma}, \tilde{\mu})$-plane. These lines and the family of ellipses are plotted in Fig. 19.

The stability of equilibria of ODE (51) is defined by the trace and the determinant of its Jacobian matrix

$$J = \begin{bmatrix} \tilde{\mu}\left(1-|v|^2\right) - 2\tilde{\mu}\left(v_R^2 - \gamma v_R v_I\right) & -\left(\tilde{\sigma} - \tilde{\mu}\gamma|v|^2\right) - 2\tilde{\mu}\left(v_R v_I - \gamma v_I^2\right) \\ \left(\tilde{\sigma} - \tilde{\mu}\gamma|v|^2\right) - 2\tilde{\mu}\left(v_R v_I + \gamma v_R^2\right) & \tilde{\mu}\left(1-|v|^2\right) - 2\tilde{\mu}\left(v_I^2 + \gamma v_R v_I\right) \end{bmatrix}: \tag{54}$$

$$\det J = \tilde{\mu}^2\left(1-|v|^2\right)\left(1-3|v|^2\right) + \left(\tilde{\sigma} - \tilde{\mu}\gamma|v|^2\right)\left(\tilde{\sigma} - 3\tilde{\mu}\gamma|v|^2\right), \tag{55}$$

$$\operatorname{tr} J = 2\tilde{\mu}\left(1-2|v|^2\right). \tag{56}$$

The condition $\operatorname{tr} J = 0$ defines the ellipse plotted in red in Fig. 19:

$$\frac{\tilde{\mu}^2}{8}(1+\gamma) - \frac{\gamma}{2}\tilde{\sigma}\tilde{\mu} + \frac{\tilde{\sigma}^2}{2} = 1. \tag{57}$$

The condition $\det J = 0$ together with Eq. (52) defines the curve plotted in Fig. 19 in magenta. This curve also bounds the region where Eq. (51) has three equilibria. The singular points, the cusps, of the $\det J = 0$ curve will be found using the singularity theory approach in the next section.

4.4 Singularity theory approach

In this section, we apply the singularity theory approach [36] to analyze the solutions to the equation

$$\left(\mu + \varepsilon - |u|^2\right)^2 |u|^2 + \left(\sigma - \gamma|u|^2\right)^2 |u|^2 = \lambda^2\mu \tag{58}$$

for the squared amplitude, $|u|^2$, of the second cell at a periodic solution to system (46). Eq. (58) is obtained from Eq. (48) by splitting it into a system of ODEs for the real and complex parts of u, $u = u_R + iu_I$, setting their right-hand sides to zero, and taking $\lambda\sqrt{\mu}$ to the left-hand side and squaring. Expanding Eq. (58) and grouping terms according to the powers of $x := |u|^2$, we obtain the following parametric cubic equation

$$G(x, \mu, \sigma, \varepsilon, \lambda, \gamma) := x^3(1+\gamma^2) - 2x^2(\mu + \varepsilon + \sigma\gamma) + x\left((\mu+\varepsilon)^2 + \sigma^2\right) - \lambda^2\mu = 0. \tag{59}$$

The singularity theory approach [36] consists of several steps. The first step is the so-called *recognition problem*, whose task is to select one parameter to be the bifurcation parameter, set the remaining parameters to zero, and identify which parametric family, i.e., which normal form, the resulting equation belongs to. The second step is to check whether the original equation, with all parameters nonzero, is a *versal unfolding* of the normal form identified in the first step. The adjective "versal" means that the parametric family contains all possible one-parameter perturbations of the normal form, thereby encompassing all perturbed bifurcation diagrams. The versal unfolding is universal if it requires the fewest additional parameters beyond the